Engineered biochar composites with zeolite, silica, and nano-zerovalent iron for the efficient scavenging of chlortetracycline from aqueous solutions

Munir Ahmad, Adel R. A. Usman, Muhammad Imran Rafique & Mohammad I. Al-Wabel

Environmental Science and Pollution Research

ISSN 0944-1344

Environ Sci Pollut Res
DOI 10.1007/s11356-019-04850-7

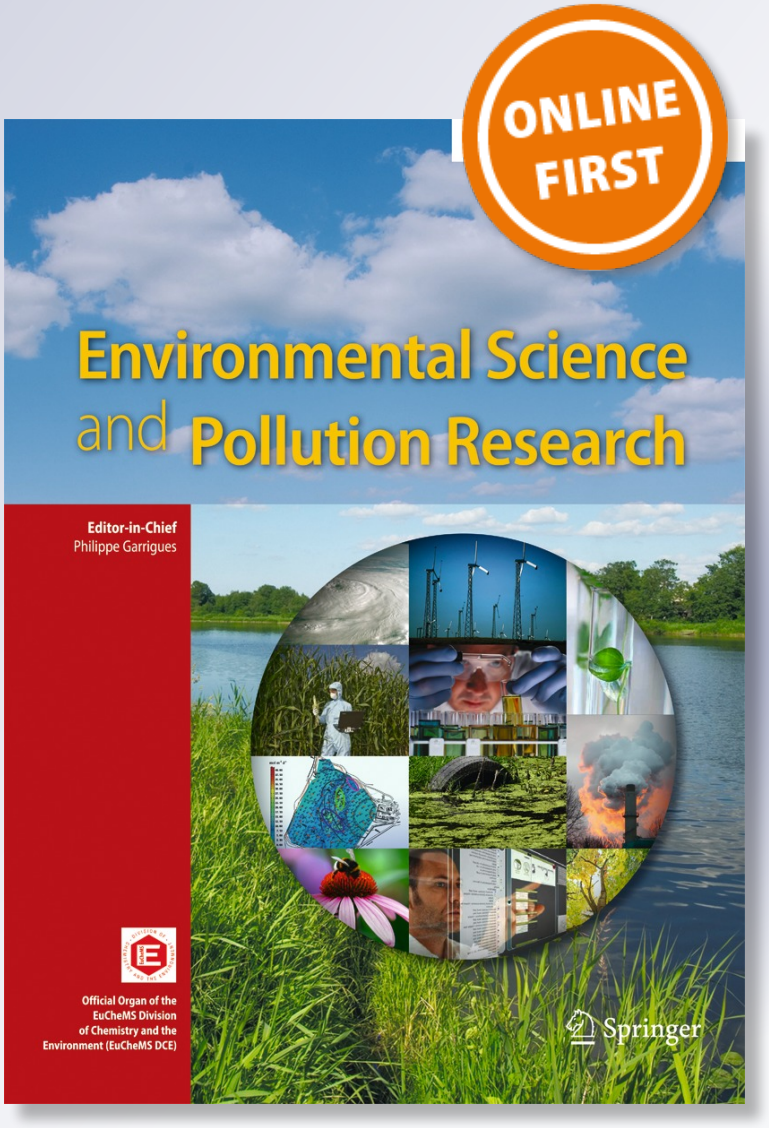

Springer

Environmental Science and Pollution Research
https://doi.org/10.1007/s11356-019-04850-7

RESEARCH ARTICLE

Engineered biochar composites with zeolite, silica, and nano-zerovalent iron for the efficient scavenging of chlortetracycline from aqueous solutions

Munir Ahmad[1] · Adel R. A. Usman[1,2] · Muhammad Imran Rafique[1] · Mohammad I. Al-Wabel[1]

Received: 23 December 2018 / Accepted: 12 March 2019

Abstract

Date palm waste–derived biochar (DBC) was produced through pyrolysis (600 °C) and modified with zeolite (Z-DBC), silica (S-DBC), or nano-zerovalent iron (nZVI-DBC) to design efficient sorbents. The pristine and engineered biochars were characterized by SEM, XRD, BET, TGA, CHNS-O, and FTIR to investigate the surface, structural, and mineralogical composition. The nZVI-DBC exhibited lowest pH (6.15) and highest surface area (220.92 $m^2\ g^{-1}$), carbon (80.55%), nitrogen (3.78%), and hydrogen (11.09%) contents compared with other biochars. Isotherm sorption data for chlortetracycline (CTC) removal from aqueous solutions was described well by Langmuir and Redlich–Peterson isotherms showing the highest fitness (R^2 values in the range of 0.88–0.98 and 0.88–0.99, respectively). Langmuir predicted maximum CTC adsorption capacity was in order of nZVI-DBC (89.05 mg g^{-1}) > S-DBC (45.57 mg g^{-1}) > Z-DBC (30.42 mg g^{-1}) > DBC (28.19 mg g^{-1}). Kinetics adsorption data was best described by power function model ($R^2 = 0.93$–0.99), followed by interaparticle diffusion ($R^2 = 0.85$–0.96) model. The nZVI-DBC performed outclass by removing 98% of CTC, followed by S-DBC (68%), Z-DBC (35%), and DBC (36%). Chemisorption, H-bonding, and interaparticle diffusion were the operating mechanisms for CTC adsorption onto DBC, S-DBC, and Z-DBC, while π-π electron donor–accepter interactions and redox reactions augmented these mechanisms for highest CTC adsorption onto nZVI-DBC. Therefore, nZVI-DBC may serve as an efficient green technology for the removal of CTC from aqueous solutions and to reduce surface date palm waste pollution.

Highlights

- Magnetic and organo-mineral biochar composites were engineered and characterized.
- nZVI-DBC has shown highest surface area and lowest pH among all biochar composites.
- nZVI-DBC exhibited three times more chlortetracycline removal than pristine biochar.
- Chemisorption, physisorption, and diffusion were sorption controlling mechanisms.
- π-π interactions and redox reactions augmented chlortetracycline sorption in nZVI-DBC.

Responsible editor: Tito Roberto Cadaval Jr

Electronic supplementary material The online version of this article (https://doi.org/10.1007/s11356-019-04850-7) contains supplementary material, which is available to authorized users.

✉ Mohammad I. Al-Wabel
malwabel@ksu.edu.sa

[1] Soil Sciences Department, College of Food & Agricultural Sciences, King Saud University, P.O. Box 2460, Riyadh 11451, Kingdom of Saudi Arabia

[2] Department of Soils and Water, Faculty of Agriculture, Assiut University, Asyut 71526, Egypt

Published online: 28 March 2019

Keywords Antibiotics · Chemisorption · Redox reactions · Removal mechanism · Surface pollution

Introduction

Antibiotics are among the most common pharmaceutical products that have been used widely from the last seven decades for both human and animals to control and prevent infectious diseases. Over 250 antibiotic types have been reported currently in use as human and veterinary medicines around the globe with an annual consumption of 63,151 ton (Ashfaq et al. 2015; Kümmerer and Henninger 2003). Due to extensive usage, antibiotics and their metabolites have been detected in various environmental matrices such as hospital wastewater (Ashfaq et al. 2015), municipal wastewater (Lindberg et al. 2010), surface water (Makowska et al. 2016), and even in drinking water (Simazaki et al. 2015), because a substantial amount of antibiotics (~ 70%) is not metabolized nor absorbed in the body of the target organism and thus excreted into the environment resulting in soil and water contamination (Kummerer 2009). The antibiotic contamination is responsible for various disorders in human beings such as allergic/anaphylactic reactions, liver injury, delayed blood coagulation, and discoloration of teeth especially in children of less than 7 years old (Singh et al. 2014).

Among the most commonly used veterinary antibiotics, chlortetracycline (CTC) is a broad spectrum antibiotic which is used for the treatment of bacterial infection and as food supplement for livestock and poultry (Bao et al. 2009). It belongs to the family tetracycline which is commonly used for animal production. Widespread use of CTC has resulted in elevated levels of its residues in soil and underground waters as > 75% of CTC remains unabsorbed and excretes out with animal manure (Montforts 1999). Applying this manure to soil as fertilizer and/or dumping this in the soil are deteriorating the ecosystem. Accumulation of CTC residues in soil and water is posing adverse ecological threats, and their concentration in plant and crop tissues is being increased with increased manure application (Kumar et al. 2005). Therefore, CTC residues are recognized as potential organic pollutants and their occurrence have been reported worldwide which needs immediate attention (Daughton and Ternes 1999). Consequently, researchers are in surge of low cost and practically feasible processes to limit antibiotics' release into soil and water, as well as to remove the prevailing antibiotics from the wastewater. Different processes have been employed to remove various antibiotics from wastewater including biological treatments, membrane separation, activated carbon, adsorption, advanced oxidation process (AOP), and chemical treatments. Among these processes, adsorption is the most accepted and widely used technique as it is inexpensive, practically easy to perform, and contains lower risk of toxicity (Hao et al. 2012; Zhou et al. 2012; Ahmaruzzaman 2008). However, the selection of appropriate adsorbent is of critical importance as the efficiency of adsorbents depends on the type of adsorbent, type of adsorbate, and composition of waste medium. Therefore, it is the dire need of time to develop new low-cost, eco-friendly, and efficient sorbents for the removal of CTC from water media.

Biochar has recently been introduced as adsorbent for the removal of toxic metal ions and organic contaminants from wastewater (Ahmad et al. 2018a). Biochar is a carbon-rich solid material produced from organic wastes through pyrolysis in controlled environment under limited oxygen supply (Aly 2017). Adsorption by using biochar is considered to be an innovative and promising practice as compared with other conventional techniques. The presence of functional groups on biochar surface, high surface area, microporous structure, diverse surface sites, and net negative charge makes biochar an efficient adsorbent for a range of organic and inorganic pollutants (Uchimiya et al. 2012; Reddy and Lee 2014). However, due to heterogeneity in structure and properties, biochar does not perform consistently. Yao et al. (2013) reported that unmodified biochar due to its low adsorption capacity and low anti-interference ability does not perform up to the mark. On the other hand, due to both positively and negatively charged surfaces (based on pyrolysis temperature), majority of the biochar possess low adsorption capability for some anionic pollutants. To conquer the abovementioned constraints, researchers are trying to modify the biochar through mechanical, chemical, and physical means to improve its efficiency for enhanced organic and inorganic pollutants' removal.

Modifications of biochar may alter its surface functional groups, surface area, surface charges, and ash contents, subsequently altering the biochar efficiency for the removal and fixation of toxic metal ions and several organic compounds. It has been reported that the adsorption of organic pollutant such as CTC can be increased by engineering a biochar with more oxygen-containing functional groups (Liu et al. 2011). Henceforth, modification of biochar may potentially improve its surface properties (hydrophobicity/hydrophilicity, surface charge, surface area, and pore volume) resulting in higher adsorption of organic pollutants. Various foreign agents such as silica, zeolite, and nano-metal oxides have been used for biochar modifications (Dong et al. 2017; Ahmad et al. 2017; Ahmad et al. 2018a). Zeolite, due to its strong electric field, larger surface area, great ion-exchange capacity, and microstructure, is a

wonderful clay mineral and is being widely used to remove pollutants from contaminated soil (Bilgic 2005; Gurses et al. 2006). Likewise, nano-sized silica possesses higher specific surface area and hydrothermal stability. Therefore, combination of biochar with zeolite and/or silica minerals may improve physiochemical properties of biochar and enhance its potential for fixation of organic and inorganic toxins in soil and water (Wang et al. 2016). Similarly, nano-zerovalent iron (nZVI) due to its nanoscale particle size, large surface area, and reductive nature has been used to remediate a range of environmental contaminants in soil and water (Chatterjee et al. 2010; Meng et al. 2006; Zhao et al. 2008; Xu et al. 2010). However, the applicability of nZVI is cumbersome due to its oxidative nature and aggregation potential (Phenrat et al. 2006; Devi and Saroha 2014). Thus, if composited with biochar, nZVI may get stabilized, consequently resulting in lower agglomeration and more feasible applicability. Therefore, modification of biochar with nZVI, silica, and/or zeolite may alter the functional groups on the surface of biochar resulting in enhanced H-bonding, covalent binding, and π-π electron donor–acceptor interactions subsequently resulting in higher adsorption (Mohan et al. 2014; Wang et al. 2017). However, up to the best of our knowledge, the efficiency of the engineered biochar composites with nZVI, silica, or zeolite for CTC adsorption has not been reported yet. Therefore, we proposed that modification of biochar using nZVI, silica, or zeolite minerals could produce efficient engineered biochars with improved adsorption characteristics. Thus, engineered biochars with nano-zerovalent iron, silica, and zeolite were produced and characterized in this study. Furthermore, the efficiency of the engineered and pristine biochars for the removal of CTC from aqueous solutions was investigated, and the operating adsorption mechanisms were investigated by employing various isotherms and kinetics models.

Materials and methods

Biochar production

Date palm tree waste was collected and washed with deionized water to remove dust and other impurities. After air drying, the leaflets were separated from the stem, cut into small pieces, grinded with a mechanical grinder, and passed through a 0.6-mm screen. This biomass was further milled in a ball mill (Fritsch Pulverisette 7, Germany) at 800 rpm for 20 min. A weighed amount of the ball-milled date palm biomass (DBM) was placed in a crucible, loosely covered, and pyrolyzed (5 °C per min) at 600 °C for 3 h in a tube furnace (Carbolite, type 3216, UK) in oxygen-limited environment. After pyrolysis, the crucible was placed in a desiccator for half an hour for cooling and to remove moisture. The weight of the produced biochar was recorded and yield was calculated using Eq. 1.

$$\text{Yield}\ (\%) = \frac{\text{weight of biomass} - \text{weight of biochar}}{\text{weight of biomass}} \times 100 \quad (1)$$

The produced biochar was washed thrice with deionized water, grinded, stored in airtight containers, and labeled as DBC.

Engineered nano-zerovalent ion–composited biochar synthesis

Date palm waste–derived biochar (DBC) was composited with nano-zerovalent iron (nZVI) by following the procedure reported by Ahmad et al. (2018a). Briefly, 100 mL of 1 M $FeSO_4.7H_2O$ solution was prepared in 4:1 (*v*/*v* ration) ethanol:deionized water solution and poured in a three-neck flask. 5.6 g of DBC was added into the flask and pH was adjusted at 5 using 5 N H_2SO_4. The suspension was stirred vigorously for 2 h initially and then purged with N_2 for 1 h during stirring. One hundred milliliters of 2 M $NaBH_4$ solution was added drop-wise into the flask under continues stirring and N_2 supply. The immediate reaction took place evolving the H_2, and black nano-zerovalent iron (Fe^0) particles started to accumulate on DBC matrix. After completion of the reaction, 1.12 g chitosan in 2% CH_3COOH solution was added. The suspension was stirred for another 30 min, and 100 mL of 1.2% NaOH solution was poured under gentle stirring. The N_2 supply was stopped; flask was air-tightened and kept overnight. The next day, the solid precipitates were separated, washed several times with ethanol to remove surplus sulfate and iron, dried in oxygen-free environment, and labeled as nZVI-DBC.

Engineered mineral-composited biochars synthesis

The DBC mineral composites were engineered according to the procedure adopted by Ahmad et al. (2017). The DBM was treated with silica and zeolite minerals prior to pyrolysis. The silica was washed with 10% HCl, 30% H_2O_2 solutions, and deionized water to remove organic matter, carbonates, and other impurities, and dried in an oven. Zeolite (clinoptilolite 25523: purchased from San Bernardino Co. PO Box. 591 Clarkson, NY) was grinded and passed through a 0.6-mm sieve. The prepared silica and zeolite minerals were milled in a ball mill at 800 rpm for 20 min. Four grams of milled silica (S) or zeolite (Z) was added into 1 L deionized water and sonicated (Sonics Vibra-Cell VCX-500 Ultrasonic Processor) for 30 min at 35 amp. The suspension was placed on a stirrer; 20 g of DBM was added and stirred for 3 h. The silica- or zeolite-impregnated biomass was separated from the

suspension and dried in an oven at 80 °C. After drying, weighed amount of solid material was placed in a crucible, loosely covered, and pyrolyzed (5 °C per min) in a tube furnace at 600 °C for 3 h in oxygen-limited environment. After the material cooled down, it was weighed to calculate yield according to Eq. 1 (after correction of silica and zeolite weights), washed thrice with deionized water, and dried in an oven. Silica- and zeolite-composited biochars were labeled as S-DBC and Z-DBC, respectively.

Characterization of engineered biochars

The proximate analyses such as moisture, volatile matter, and ash contents in the biochars were determined by the standard methods provided by ASTM D1762-84 (ASTM 1989), whereas the resident matter (fixed carbon) was calculated using the difference method. The pH of the biochars was determined in 1:10 (*w*/*v* ratio) of material to deionized water suspension. Cation exchange capacity (CEC) was measured using the method described by Richard (1954). The pH at point of zero charge (pH_{PZC}) was estimated by using 0.01 M NaCl in an initial pH range of 2–12 (Usman et al. 2015).

The scanning electron microscope (SEM; EFI S50 Inspect, Netherlands) was used to observe the structural changes and surface morphology of the biochars. Briefly, a few particles of the material were scattered on the aluminum stubs coated with adhesive carbon tape (12 mm; PELCO, UK) and coated with nano-gold particles for 60 s via 108 Auto/SE Sputter Coater (Ted Pella Inc., USA). Images of the material were taken with different magnifications at 30 kV voltage under high vacuum. The thermogravimetric analyzer (TGA-DTG-60H, Shimadzu, Japan) was used to analyze the thermal stability of the biochars in a temperature range of 0–1100 °C. The Fourier transform infrared spectroscopy (FTIR; Bruker Alpha-Eco ATR-FTIR, Bruker Optics Inc.) was used to observe the composition of structural and functional groups in the biochars. X-ray diffractometer (MAXima_X XRD-7000, Shimadzu, Japan) was used to analyze the mineralogical phases of the produced biochars. The Brunauer–Emmett–Teller (BET; TriStar II 3020, Micromeritics, USA) method was used to analyze the surface area, total pore volume, and pore diameter. The CHNSO elemental analyzer (series II, PerkinElmer, USA) was used to assess the elemental composition. The percent carbon (C), nitrogen (N), hydrogen (H), and sulfur (S) content was analyzed with the CHNSO analyzer directly, while oxygen (O) was calculated using Eq. 2 and atomic ratios of O/C and H/C were calculated.

$$\mathrm{O}\ (\%) = 100 - [\mathrm{C}\ (\%) + \mathrm{H}\ (\%) + \mathrm{N}\ (\%) + \mathrm{S}\ (\%) + \mathrm{ash}\ (\%)] \quad (2)$$

Equilibrium adsorption experiments

Date palm–derived biochar and its composites were tested for their efficiency to remove chlortetracycline (CTC) from the aqueous solution by isotherm sorption batch-type experiments. A stock solution containing 500 mg CTC L^{-1} was prepared in methanol, which was further diluted in deionized water (18.2 MΩ cm^{-1} resistivity; Milli-Q, Germany) to prepare working solutions of 0, 5, 10, 20, 50, and 100 mg CTC L^{-1}. The pH of the working solution was adjusted at 5 using HCl and NaOH. Twenty-five milliliters of each working solution was added into polypropylene conical tubes, and the produced materials were suspended separately in tubes at the rate of 1 g L^{-1}. After shaking at 150 rpm for 24 h at room temperature (23 ± 2 °C), the solutions were filtered by 0.45 μm syringe filters. Three replications of each biochar including a blank were performed. The equilibrium concentration of CTC in the solution was analyzed by high-performance liquid chromatography (HPLC; Prominence-*i*, LC-2030C, Shimadzu, Japan), equipped with an auto-sampler (high-speed drive LC-2030), a PDA detector, a pump (low-pressure gradient solvent delivery LC-2030), and a degasser unit. The equipment was also equipped with a reversed-phase Raptor C18 column (100 mm × 21 mm, 2.7 μm particle size, Restek Corporation, USA). The mobile phase A consisted of ultrapure water and formic acid solution (99.9:0.1 *v*/*v* ratio), while the mobile phase B consisted of HPLC grade acetonitrile and formic acid (99.9:0.1 *v*/*v* ratio). The gradient flow consisted of 70% of mobile phase A and 30% of mobile phase B. The CTC was detected at 254 nm wavelength with a flow rate of 0.15 mL min^{-1} and a total injection volume of 10 μL. The calibration curve of CTC concentration versus absorbance was developed by using analytical grade CTC standards between the ranges of 0 and 20 mg L^{-1}. The R^2 obtained from the calibration curves was > 0.98. For quality assurance, CTC standards were fed as unknown samples and observed that the recovery was 94.87–103.25%.

The amount of CTC sorbed onto the material was calculated using Eq. 3 (Ok et al. 2007).

$$q_e = \left[\frac{C_o - C_e}{m}\right] \times v \quad (3)$$

where C_o and C_e are the initial and equilibrium concentrations of CTC (mg L^{-1}), q_e is the amount of CTC sorbed (mg g^{-1}), m is the mass of material (g), and v is the volume of solution (L).

To investigate the efficiency of the biochars for the adsorption of CTC, nonlinear forms of the Freundlich, Langmuir, Redlich–Peterson, Temkin, and Dubinin–Radushkevich

equations (Eqs. 4, 5, 6, 7, and 8, respectively) were applied (Ahmad et al. 2013; Redlich and Peterson 1959).

$$q_e = K_F C_e^{1/n} \tag{4}$$

$$q_e = \frac{Q_L C_e K_L}{1 + K_L C_e} \tag{5}$$

$$q_e = \frac{AC_e}{1 + BC_e^g} \tag{6}$$

$$q_e = \frac{RT}{b} \ln(AC_e) \tag{7}$$

$$q_e = q_D \exp\left(-B_D \left[RT \ln\left(1 + \frac{1}{C_e}\right)\right]^2\right) \tag{8}$$

where K_F is the Freundlich sorptive affinity parameter (L g^{-1}), $1/n$ is the Freundlich component related to linearity, Q_L is the Langmuir maximum adsorption capacity (mg g^{-1}), K_L is the Langmuir sorption equilibrium constant (L mg^{-1}), A and B are the Redlich–Peterson equation constant (L g^{-1} and (L $mg^{-1})^g$, respectively), and g is the exponent having the value between 0 and 1. A is the binding constant (L mg^{-1}), b is the heat of adsorption, q_D is the maximum adsorption capacity of the adsorbent (mg g^{-1}), and B_D is the mean free energy of sorption used to calculate the bonding energy (E) for the ion-exchange mechanism according to Eq. 9.

$$E = \frac{1}{\sqrt{2B_D}} \tag{9}$$

Langmuir separation factor (R_L), as given in Eq. 10, was used to assess the favorability of CTC adsorption onto the biochars.

$$R_L = \frac{1}{1 + K_L C_o} \tag{10}$$

The coefficient of determination (R^2) was calculated by using Eq. 11 to determine the closeness between the experimental adsorption data and the model predicted data (Ahmad et al. 2018b).

$$R^2 = \frac{\left(q_{em} - \overline{q_{ec}}\right)^2}{\sum\left(q_{em} - \overline{q_{ec}}\right)^2 + \left(q_{em} - q_{ec}\right)^2} \tag{11}$$

where q_{ec} and q_{em} are the calculated and measured amounts of CTC sorbed (mg g^{-1}) onto the biochars at equilibrium.

Kinetics adsorption experiments

Kinetics adsorption experiments were conducted to investigate the rate of CTC adsorption onto the produced biochars. A working solution containing 100 mg CTC L^{-1} was prepared in deionized water using the stock solution (500 mg L^{-1} in methanol), and the pH was adjusted at 5. The biochars were suspended in 25 mL of the working solution in a polypropylene conical flask at the rate of 1 g L^{-1}, and shaken on a mechanical shaker at 150 rpm at room temperature (23 ± 2 °C). The mixtures were withdrawn from the shaker after 0, 60, 120, 180, 360, and 720 min, and the solutions were separated from the biochars and filtered through 0.45 μm syringe filters. Three replications of each material and a control (without biochars) were also included. The concentration of CTC in the filtrates was analyzed by HPLC. Amount of CTC sorbed onto per unit mass of the material was calculated using Eq. 3. The CTC removal percentage was calculated by using Eq. 12.

$$\text{Removal}\% = \left[\frac{C_o - C_t}{C_o}\right] \times 100 \tag{12}$$

To predict the mechanism for CTC adsorption onto the DBC and engineered composites (nZVI-DBC, S-DBC, and Z-DBC), various kinetic models such as first-order, second-order, pseudo-first-order, pseudo-second-order, Elovich, power function, and intraparticle diffusion (Eqs. 13, 14, 15, 16, 17, 18, and 19, respectively) were applied (Ahmad et al. 2018b).

$$\ln q_t = \ln q_o - k_1 t \tag{13}$$

$$\frac{1}{q_t} = \frac{1}{q_o} - k_2 t \tag{14}$$

$$\ln(q_e - q_t) = \ln q_e - k_1' t \tag{15}$$

$$\frac{t}{q_t} = \frac{1}{k_2' q_e^2} + \frac{1}{q_e} t \tag{16}$$

$$q_t = \frac{1}{\beta} \ln(\alpha\beta) + \frac{1}{\beta} \ln t \tag{17}$$

$$\ln q_t = \ln b + k_f (\ln t) \tag{18}$$

$$q_t = c + k_{id} t^{0.5} \tag{19}$$

where q_t and q_o are the amounts of CTC sorbed (mg g^{-1}) at time t and time 0 (min), respectively, t is the time interval, k_1 and k_2 are the first- and second-order rate constants, respectively, q_e is the adsorption capacity at equilibrium (mg g^{-1}), k_1' and k_2' are the pseudo-first- and pseudo-second-order rate constants, respectively, α is the initial adsorption rate (mg g^{-1} min^{-1}), β is the adsorption constant, b is the rate constant, k_f is the rate coefficient value (mg g^{-1} min^{-1}), k_{id} is the apparent diffusion rate constant (in [mg g^{-1}]$^{-0.5}$), and c is the diffusion constant.

The standard error of estimate (SEE) and the coefficient of determination (R^2) were calculated by using Eqs. 11 and 20, respectively, to determine the closeness between the experimental adsorption data and the model predicted data (Ahmad et al. 2018b).

$$\mathrm{SEE} = \sum_{i=1}^{n}(q_{em}-q_{ec})^2 \quad (20)$$

where q_{em} and q_{ec} are the measured and calculated CTC adsorption capacities (mg g^{-1}) of the biochars, and n is the number of measurements.

Results and discussion

Characterization

Proximate, chemical analyses, surface area, and elemental composition

Proximate composition, elemental composition, chemical analyses, and surface area analyses of the date palm waste–derived biochar and its derived composites are presented in Table 1. After excluding the contribution of the mineral silica and zeolite, S-DBC and Z-DBC exhibited 37% and 32% more yield compared with DBC, suggesting that the mineral composites of biochar were more resilient to thermal decomposition. The moisture contents reduced with pyrolysis from 4.77% in DBM to 1.58% in DBC due to volatilization and thermalization, which further reduced to 0.73% and 0.00% in S-DBC and Z-DBC, respectively, while increased in nZVI-DBC. The volatiles were reduced from 66.36% in DBM to 10.05% in DBC. The nZVI-DBC composite showed the highest volatiles among all the composites, i.e., 18.88%, while the lowest were exhibited by S-DBC followed by Z-DBC (7.59% and 10.87%, respectively). The volatiles are generally considered as an indication of biochar stability (Usman et al. 2015); therefore, lower volatiles in S-DBC suggested higher stability of this composite.

It was interesting to notice that fixed carbon contents increased with pyrolysis from 20.50% in DBM to 50.10% in DBC, which further increased to 24.91% and 31.22% in Z-DBC and S-DBC, respectively (excluding the contents of the silica and zeolite minerals), while it reduced to 10.64% when composited with nZVI. The lowest fixed carbon might be due to the presence of graphene and Fe_3C contents in nZVI-DBC composite which remained undecomposed and therefore were confused with the ash contents. The ash contents increased with pyrolysis from 8.36% in DBM to 38.27% in DBC, which further increased to 60.87%, 60.46%, and 64.22% in nZVI-DBC, S-DBC, and Z-DBC, respectively (excluding the contents of silica and zeolite minerals in S-DBC and Z-DBC composites, respectively). It has already been established that the ash contents increased with pyrolysis, due to formation and/or condensation of mineral compounds (Ozcimen and Ersoy-Mericboyu 2010; Sun et al. 2014). The pH of the

Table 1 Proximate, chemical, surface area, pore size, and pore volume analyses and elemental composition with their molar ratio results of date palm tree leaves waste biomass and its derived biochars

Parameters	Unit	DBM	DBC	nZVI-DBC	S-DBC	Z-DBC
Yield	%	–	31.78 ± 4.78	–	43.54 ± 2.27	41.83 ± 4.27
Moisture	%	4.77 ± 0.03	1.58 ± 0.75	3.96 ± 0.08	0.73 ± 0.10	0.00 ± 0.00
Volatiles	%	66.36 ± 5.53	10.05 ± 1.49	18.88 ± 1.23	7.590 ± 0.21	10.87 ± 1.28
Fixed carbon	%	20.50 ± 5.72	50.10 ± 0.98	10.64 ± 3.51	31.22 ± 0.32	24.91 ± 1.37
Ash	%	8.360 ± 0.21	38.27 ± 1.26	60.87 ± 7.31	60.46 ± 0.02	64.22 ± 0.09
pH	1:10	5.95 ± 0.03	10.1 ± 0.02	6.15 ± 0.02	8.85 ± 0.04	9.37 ± 0.01
Cation exchangeable capacity	cmol kg^{-1}	66.01 ± 0.00	57.83 ± 13.26	72.55 ± 3.95	41.27 ± 0.84	86.43 ± 0.65
Surface area	m^2 g^{-1}	0.393	198.36	220.92	124.73	134.77
Pore size	nm	28.42	5.614	5.819	6.023	9.843
Total volume in pores	cm^3 g^{-1}	0.00021	0.1069	0.06082	0.054	0.06075
C	%	41.21	75.59	8055	74.64	73.03
H	%	7.23	4.89	11.09	1.35	13.36
N	%	2.89	0.00	1.38	0.00	0.00
O	%	48.67	19.51	4.19	24.01	13.61
S	%	0.00	0.00	0.00	0.00	0.00
O/C	–	0.89	0.19	0.043	0.24	0.14
H/C	–	2.09	0.77	1.64	0.22	2.18

DBM, date palm waste biomass; *DBC*, date palm waste–derived biochar; *nZVI-DBC*, date palm waste–derived biochar composite with nano-zerovalent iron; *S-DBC*, date palm waste–derived biochar composite with silica; *Z-DBC*, date palm waste–derived biochar composite with zeolite

DBM (5.95) increased almost twofold in DBC (10.10), while 3 and 4 unite in S-DBC and Z-DBC, respectively, with pyrolysis due to lower acid functional groups and condensation of basic functional groups (Ahmad et al. 2018c). However, the pH of the composites was lower than that of the DBC. The lowest pH of nZVI-DBC (6.15) could be due to several washings which were performed during its synthesis, which might have washed out all the soluble basic cations (Ahmad et al. 2017). The CEC of the DBM reduced from 66.01 cmol kg^{-1} to 57.83 and 41.27 cmol kg^{-1} in DBC and S-DBC, respectively. This reduction in CEC might be due to loss of surface functional groups and increased carbon aromaticity during pyrolysis (Joseph et al. 2010). The highest CEC was noticed in Z-DBC (86.43 cmol kg^{-1}), followed by nZVI-BC (72.55 cmol kg^{-1}) composites, which might be due to the presence of zeolite and nanoscale iron particles in the matrix, respectively (Ahmad et al. 2017)

Surface area, pore size, and pore volume analyses results of the biochars have also been shown in Table 1. The nZVI-DBC showed the highest BET surface area (220.92 m^2 g^{-1}) among all the biochars, followed by DBC (198.36 m^2 g^{-1}), while S-DBC and Z-DBC exhibited lowest surface area (124.73 and 134.77 m^2 g^{-1}, respectively) compared with DBC alone. The highest surface area of nZVI-DBC was due to the presence of Fe^0 particles in the biochar matrix, while the lower surface area of S-DBC and Z-DBC was due to the blockage of pores in the biochar matrix with silica and zeolite particles (Ahmad et al. 2017, 2018a). Pore size reduced from 28.420 nm in DBM to ~ 5–10 nm in biochars due to condensation of aromatic structure and loss of volatiles. The total volume in pores was lower in the composite biochars (0.06082, 0.0500, and 0.06075 cm^3 g^{-1} in nZVI-DBC, S-DBC, and Z-DBC, respectively) compared with the biochar (0.10690 cm^3 g^{-1}). The reduction in the pore volume in the composite biochars could be due to the blockage of mesopores with Fe^0, silica, and zeolite particles (Rawal et al. 2016). The elemental composition of the biochars showed that the carbon (C) contents increased with the pyrolysis from 41.21% in DBM to 75.59% in DBC due to carbonization. It was interesting to observe that the C contents in S-DBC and Z-DBC remained comparable (74.64% and 73.03%, respectively) to that in DBC, while increased slightly in nZVI-DBC (80.55%). The contents of H reduced with pyrolysis in DBC and S-DBC, while increased in Z-DBC and nZVI-DBC, which could be due to the bonding of H with minerals. Likewise, the N and O contents reduced with thermalization of the DBM, which could be due to loss of the functional groups as a result of dehydration and depolymerization (Al-Wabel et al. 2013). The O/C molar ratios indicated that all biochar-based materials possess the lower values compared with DBM, suggesting a decrease in hydrophobicity and surface polarity with pyrolysis. The lowest H/C molar was exhibited by S-DBC, suggesting the higher aromatic nature of the composite (Usman et al. 2015). The surface polarity and aromaticity of the biochar-based composites have been presented with van Krevelen diagram (Fig. S1 in the Supplementary Material), indicating that the biochar-based materials possessed lower O/C ratios suggesting higher stability than the DBM.

Ultimate analyses

The surface morphology as indicated by the SEM images (Fig. 1a–e) represented the formation of channelized surface of the biochar composites as a result of pyrolysis. The rod-like structures on nZVI-DBC represented the presence of Fe^0 particles onto biochar matrix, while the presence of silica and zeolite mineral particles was also observed on the surface of S-DBC and Z-DBC, respectively. The variation in the mineralogical phases of the biochars was investigated with XRD (Fig. 2a, b). A sharp peak in DBM at $2\theta = 21.48$ was designated as mellite ($Al_2[C_6(COO)_6].16H_2O$), which reduced to its minimum in all the composited biochars. Likewise, the peaks ascribed as calcite ($CaCO_3$) and sylvite (KCl) in DBM were also reduced after pyrolysis. The peaks at $2\theta = 44$ and 63 in nZVI-DBC confirmed the presence of Fe^0 particles (Ahmad et al. 2018a). A small peak of graphene was also detected at $2\theta = 18.5$ in nZVI-DBC. The peaks at $2\theta = 9.82$, 11.14, 19.06, and 22.29 were designated as clinoptilolite (zeolite) in Z-DBC. The peaks at $2\theta = 20.88$ and 26.68 were designated as SiO_2, while a peak at $2\theta = 50.18$ was designated as feldspar in S-DBC. The FTIR spectra of the synthesized composites are presented in Fig. 2c. A broad band in DBM at 3300 cm^{-1} was ascribed as O–H stretches of H-bonding of the water molecules, which vanished with pyrolysis. Likewise, two bands around 2900 cm^{-1} in DBM were designated as O–H and aliphatic C–H stretches, which were lost during pyrolysis. A band at 1089 cm^{-1} in all the biochars (except nZVI-DBC) was due to C–O–C stretches (polysaccharide cellulose). The bands around 3300 and 1625 cm^{-1} in nZVI-DBC were due to N–H stretches (due to the presence of chitosan). The presence of Fe^0 nanoparticles in nZVI-DBC was confirmed with a sharp band at 3426 cm^{-1} due to the presence of stretching vibration of –OH, suggesting the formation of ferric oxyhydroxide (FeOOH) layer on Fe^0 nanoparticles (Singh et al. 2011). A band at 777 cm^{-1} in S-DBC was ascribed as Si–O. A band representing clinoptilolite $(Na, K, Ca)_{2-3}Al_3(Al,Si)_2Si_{13}O_{36}.12H_2O$ due to TO_4 (tetrahedral) of Al–Si was overlapped at 1089 cm^{-1} in Z-DBC. Thermal degradability of the biochars as assessed through TGA thermograms is presented in Fig. S2. Weight loss around 200 °C was due to the loss of non-structural free water, while from 300 to 400 °C was due to the decomposition of cellulosic and hemicellulosic compounds (Yang et al. 2007). The complete weight loss due to the degradation of lignin occurred around 650–800 °C for nZVI-DBC, S-

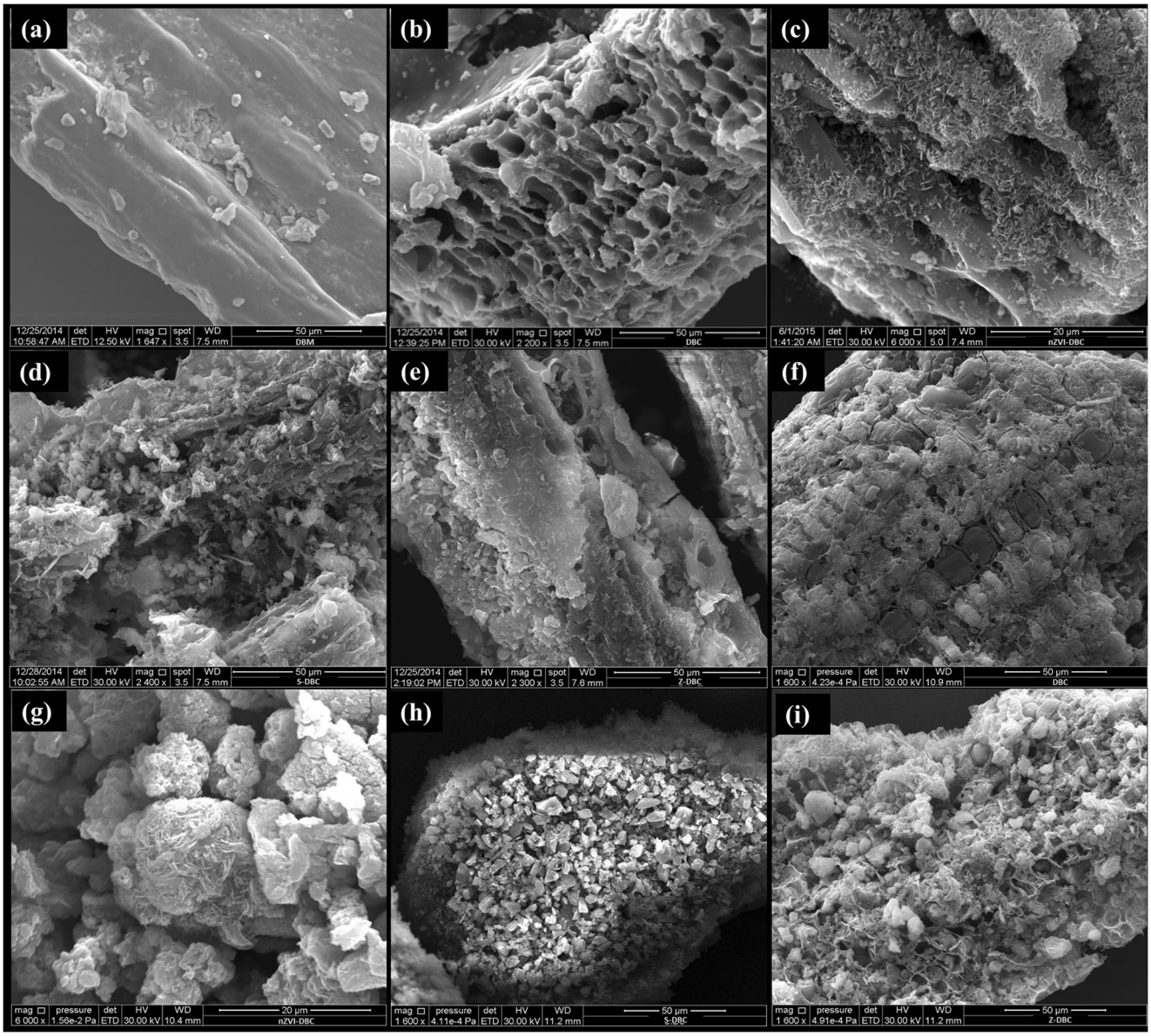

Fig. 1 Scanning electron microscope (SEM) images of **a** date palm waste–derived biomass (DBM), **b** date palm waste–derived biochar (DBC), **c** date palm waste–derived biochar composite with nano-zerovalent iron (nZVI-DBC), **d** date palm waste–derived biochar composite with silica (S-DBC), **e** date palm waste–derived biochar composite with zeolite (Z-DBC), **f** date palm waste–derived biochar (DBC) after CTC (chlortetracycline) adsorption, **g** date palm waste–derived biochar composite with nano-zerovalent iron (nZVI-DBC) after CTC adsorption, **h** date palm waste–derived biochar composite with silica (S-DBC) after CTC adsorption, and **i** date palm waste–derived biochar composite with zeolite (Z-DBC) after CTC adsorption

DBC, and Z-DBC, while at 900 and 1010 °C for DBM and DBC, respectively (Hernandez-Mena et al. 2014).

Equilibrium CTC adsorption

The efficacy of the engineered and pristine biochars for CTC adsorption was evaluated in equilibrium batch adsorption experiments. The nonlinear forms of Langmuir, Freundlich, Temkin, Dubinin–Radushkevich, and Redlich–Peterson isotherms were employed to evade the errors, and the resultant adsorption isotherms are presented in Fig. 3. It is obvious in all the isotherms that the CTC adsorption increased with increase in initial solution concentration until equilibrium (Ahmad et al. 2018a, b). The nZVI-DBC exhibited H-type (high-affinity) isotherm suggesting a strong adsorbent-adsorbate interactions, while the other sorbents demonstrated L-type isotherm suggesting less availability of the active sites (Ahmad et al. 2018b). Overall, the five isotherms presented a similar trend for CTC adsorption following the order of nZVI-DBC > S-DBC > Z-DBC > DBC. The isotherm parameters obtained from nonlinear regressions are provided in Table 2. All the employed models exhibited good fitness with $R^2 > 0.78$;

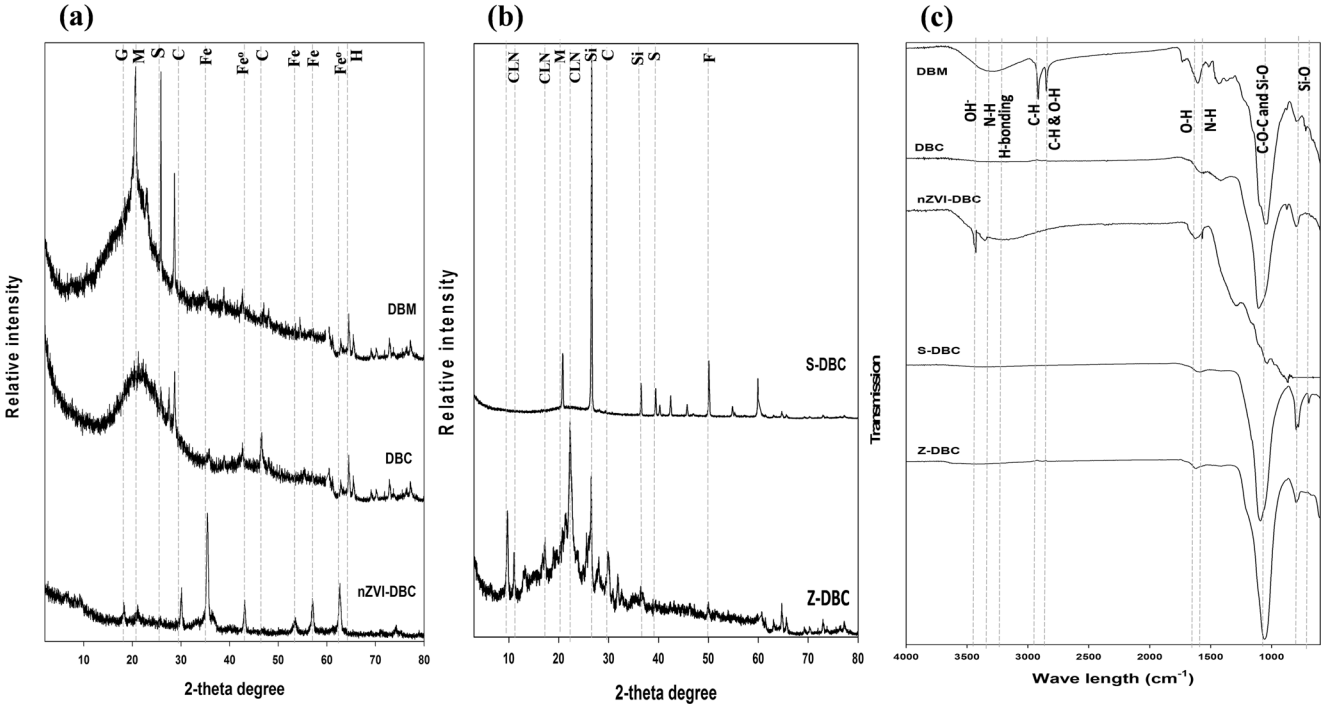

Fig. 2 X-ray diffraction patterns (**a** and **b**) and Fourier transform infrared spectroscopy spectra (**c**) of DBC (date palm waste–derived biochar), nZVI-DBC (date palm waste–derived biochar composite with nanozerovalent iron), S-DBC (date palm waste–derived biochar composite with silica), and Z-DBC (date palm waste–derived biochar composite with zeolite) (G: graphene, M: mellite, S: sylvite, C: calcite, H: halite)

however, the Langmuir and Redlich–Peterson isotherms showed the highest fitness to the adsorption data by generating the highest R^2 values in the range of 0.88–0.98 and 0.88–0.99, respectively, compared with the rest of the isotherms. The Langmuir isotherm–predicted maximum CTC adsorption capacities (Q_L) of the engineered biochars were 89.05, 45.57, 30.42, and 28.19 mg g^{-1} for nZVI-DBC, S-DBC, Z-DBC, and DBC, respectively, suggesting the nZVI-DBC as the most efficient sorbent for CTC among the tested biochars. The Freundlich isotherm–predicted sorptive affinity (K_F) followed the same order giving the highest value for nZVI-DBC (25.665 L g^{-1}), followed by S-DBC (17.005 L g^{-1}), Z-DBC (12.310 L g^{-1}), and DBC (8.146 L g^{-1}), suggesting the highest adsorption onto nZVI-DBC due to the greater availability of adsorption sites.

As the Redlich–Peterson equation integrates the features of both Freundlich and Langmuir, it can be employed either for heterogeneous or homogenous systems (Foo and Hameed 2010). The best fit of the Redlich–Peterson model also suggested that multiple mechanisms were involved in the CTC adsorption onto engineered biochars (Liu et al. 2010). The Redlich–Peterson-predicted g values were in the range of 0.533–0.992, suggesting that the imitation for Langmuir isotherm was more than Freundlich. The nZVI-DBC showed the lowest value of g, suggesting higher CTC adsorption, which is also in agreement with Langmuir and Freundlich isotherms. The higher heat of adsorption (b) as predicted by Temkin isotherm was seen in the case of nZVI-DBC (12.536 J mol^{-1}), followed by S-DBC (6.476 J mol^{-1}), Z-DBC (4.688 J mol^{-1}), and DBC (3.155 J mol^{-1}). Furthermore, the Dubinin–Radushkevich-predicted maximum CTC adsorption capacities (Q_D) were highest for nZVI-DBC (72.369 mg g^{-1}), followed by S-DBC (40.941 mg g^{-1}), Z-DBC (29.430 mg g^{-1}), and DBC (24.569 mg g^{-1}), while the bonding energies (E) for all the engineered biochars were less than 8 kJ g^{-1}. Further, the favorability for the adsorption of CTC onto the engineered biochars was tested with the help of Freundlich-predicted $1/n$ (component related to linearity) and Langmuir-predicted R_L (separation factor). It has been established that $R_L = 0$ indicates irreversible, $0 < R_L < 1$ indicates favorable, $R_L = 1$ indicates linear, and $R_L > 1$ indicates unfavorable isotherm (Mohan et al. 2011). In the current study, the R_L values ranged from 0.008 to 0.547 suggesting a favorable adsorption of CTC onto the engineered biochars (Fig. S3). It was noticed that any increase in initial CTC concentrations has resulted in reduction of R_L values. Specifically, the calculated R_L values for tested initial concentrations were in the range of 0.026–0.340, 0.016–0.243, 0.008–0.141, and 0.058–0.547 for nZVI-DBC, S-DBC, Z-DBC, and DBC, respectively. It is clear from the presented results that R_L values for all the biochars were less than unity, suggesting a favorable adsorption process. Likewise, $1/n$ ranged between 0.249 and 0.484 for all the biochars, suggesting that the sorptive affinity was favorable for the adsorption of CTC onto all the tested biochars due to the strong bonding of CTC and sorbents (Ahmad et al.

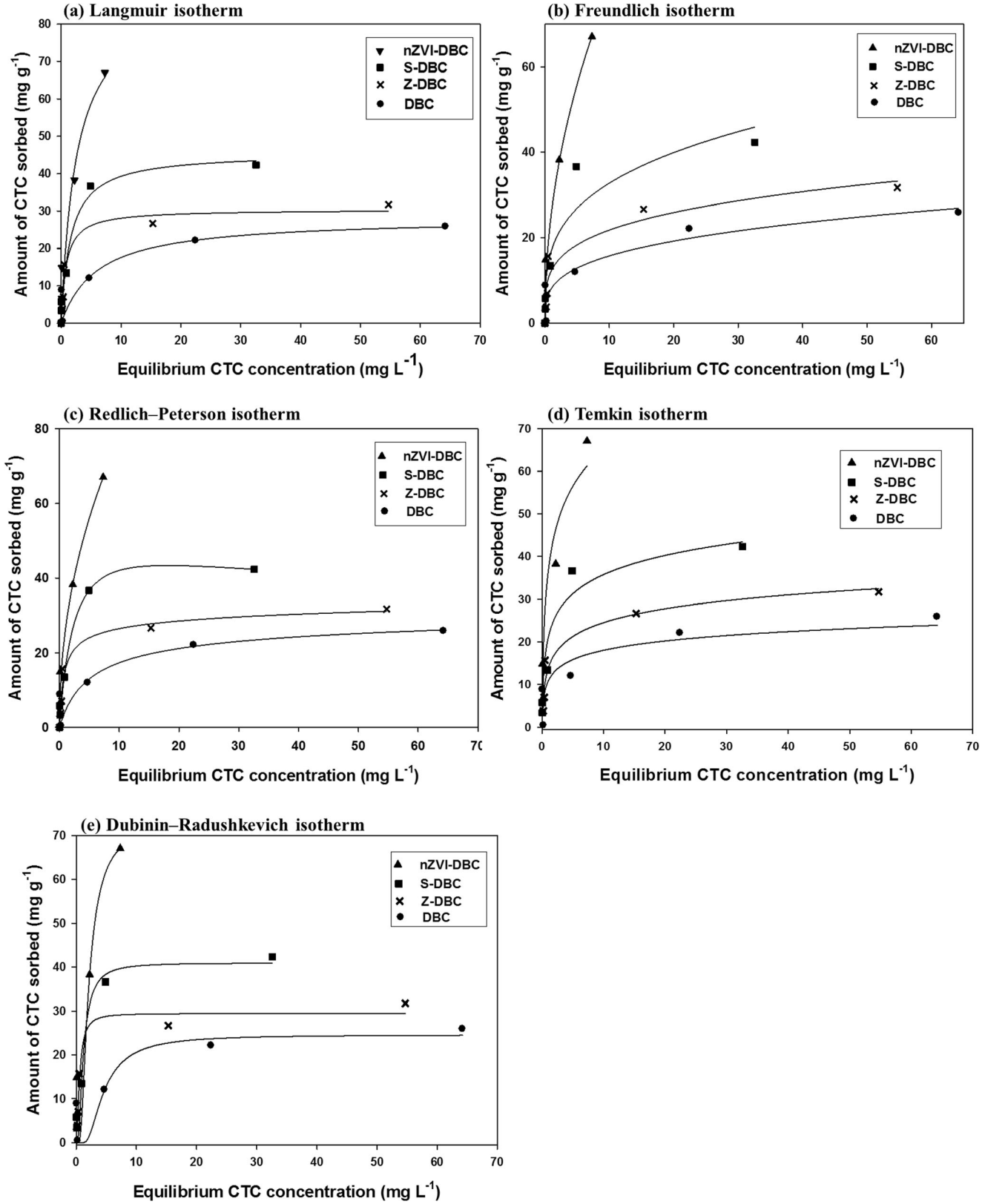

Fig. 3 CTC (chlortetracycline) adsorption isotherms fittings on **a** Langmuir, **b** Freundlich, **c** Redlich–Peterson, **d** Temkin, and **e** Dubinin–Radushkevich models by date palm waste–derived biochar (DBC), date palm waste–derived biochar composite with nano-zerovalent iron (nZVI-DBC), date palm waste–derived biochar composite with silica (S-DBC), and date palm waste–derived biochar composite with zeolite (Z-DBC)

Table 2 Nonlinear parameters of Langmuir, Freundlich, and Redlich–Peterson isotherms indicating CTC (chlortetracycline) adsorption onto date palm waste–derived biochar (DBC), date palm waste–derived biochar composite with nano-zerovalent iron (nZVI-DBC), date palm waste–derived biochar composite with silica (S-DBC), and date palm waste–derived biochar composite with zeolite (Z-DBC)

Isotherms	Parameters	nZVI-DBC	S-DBC	Z-DBC	DBC
Langmuir	Q_L (mg g^{-1})	89.05	45.57	30.42	28.19
	K_L (L g^{-1})	0.388	0.624	1.219	0.165
	R^2	0.96	0.98	0.96	0.88
Freundlich	K_F (L g^{-1})	25.664	17.005	12.310	8.146
	$1/n$	0.484	0.285	0.249	0.287
	R^2	0.98	0.91	0.92	0.90
Redlich–Peterson	A (L g^{-1})	0.304	21.884	40.812	5.514
	B (L $mg^{-1})^g$	49.820	0.304	1.812	0.255
	g	0.533	0.992	0.929	0.913
	R^2	0.98	0.99	0.96	0.88
Temkin	b (J mol^{-1})	12.536	6.476	4.688	3.155
	A (L g^{-1})	18.174	25.017	18.663	30.403
	R^2	0.94	0.94	0.94	0.78
Dubinin–Radushkevich	Q_D (mg g^{-1})	72.369	40.941	29.430	24.569
	E (kJ g^{-1})	0.0019	0.0008	0.0003	0.008
	R^2	0.90	0.96	0.96	0.80

2018a, b). These results suggested that all the investigated biochars were suitable for the removal of CTC from aqueous solutions. The nZVI-DBC was found to be the most efficient engineered biochar with highest CTC adsorption efficiency.

Kinetics CTC adsorption

Kinetics sorption batches were performed at a constant temperature to investigate the rate of CTC adsorption onto the engineered biochars, and the dynamics of adsorption are presented in Fig. 4. Three adsorption stages, i.e., rapid, relatively slow, and equilibrium, are obvious in the dynamics of CTC adsorption. The rapid adsorption stage exhibited the highest CTC adsorption during initial 180 min, by removing 90%, 43%, 30%, and 21% CTC through nZVI-DBC, S-DBC, Z-DBC, and DBC, respectively. During the relatively slow stage (180 to 360 min), nZVI-DBC, S-DBC, Z-DBC, and DBC removed 97%, 63%, 29%, and 28% of CTC, respectively. The nZVI-DBC was found to be the most efficient sorbent removing 98% CTC, followed by S-DBC (68%), Z-DBC (35%), and DBC (36%) after 360 min (equilibrium stage). The kinetics adsorption data was subjected to kinetics models such as first-order, second-order, pseudo-first-order, pseudo-second-order, Elovich, power function, and intraparticle diffusion. The estimated error functions of these models (Table 3) indicated their appropriateness for the adsorption of CTC onto the tested biochars (except first- and second-order). Based on the R^2 values, power function, intraparticle diffusion, and Elovich were the most appropriate, while first- and second-order were inappropriate models for CTC adsorption onto the tested biochars. However, pseudo-first-order and pseudo-second-order models were more appropriate for S-DBC, Z-DBC, and DBC compared with nZVI-DBC. Likewise, SEE was found to be the lowest for power function, intraparticle diffusion, Elovich, pseudo-first-order, and pseudo-second-order models compared with first- and second-order models. The parameters derived from the kinetics models are presented in Table 4. The nZVI-DBC exhibited highest rate constant ($b = 0.20$), followed by Z-DBC (0.11), S-DBC (0.05), and DBC (− 0.19) as predicted by power function. Likewise, the highest diffusion constant (c) was demonstrated by nZVI-DBC (8.88), followed by Z-DBC (3.15), S-DBC (0.10), and DBC (− 1.68). Elovich-predicted rate constant (β) was highest for S-DBC (− 6.51) followed by nZVI-DBC (− 5.13). As the rate constants determine the time for a reaction completion, therefore, highest rate constants of nZVI-DBC suggested that it required shorter time to sorb CTC compared with the other tested biochars. The initial adsorption rates as predicted by pseudo-second-order (h) and Elovich (α) models have followed the similar trend by generating the highest value for nZVI-DBC (5.76 and 11.5 mg g^{-1} min^{-1}, respectively), followed by S-DBC (0.44 and 7.80 mg g^{-1} min^{-1}, respectively), Z-DBC (0.44 and 3.84 mg g^{-1} min^{-1}, respectively), and DBC (0.13 and 2.41 mg g^{-1} min^{-1}, respectively). The maximum adsorption capacities (q_e) were in the order of nZVI-DBC, S-DBC, Z-DBC, and DBC, which were in correspondence with the Langmuir and Freundlich isotherms.

The rate coefficient (k_f) values as estimated from power function model were highest for nZVI-DBC (0.70 mg g^{-1} min^{-1}), followed by S-DBC (0.63 mg g^{-1} min^{-1}), Z-DBC (0.52 mg g^{-1} min^{-1}), and DBC (0.51 mg g^{-1} min^{-1}), suggesting increase in CTC adsorption onto these biochars with time. Similar to other parameters, the

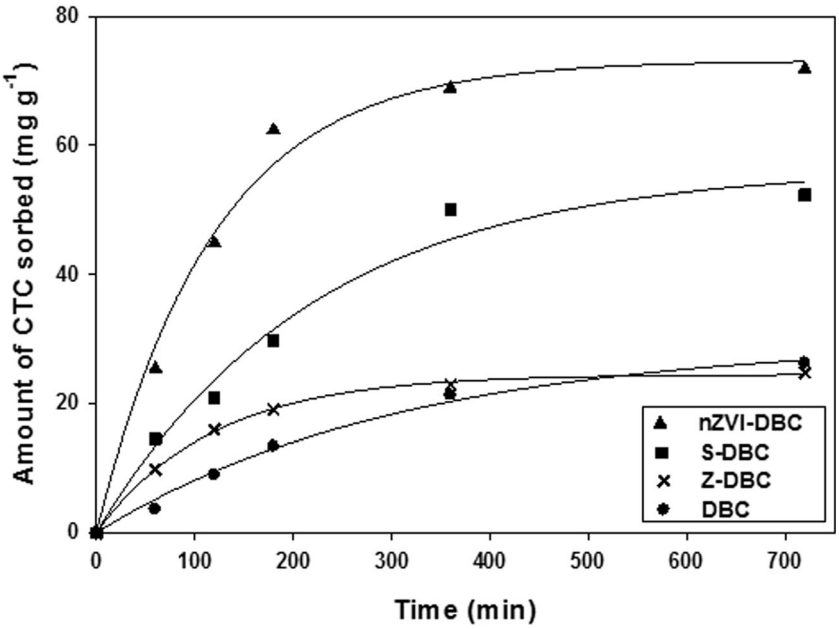

Fig. 4 CTC (chlortetracycline) adsorption kinetics onto date palm waste–derived biochar (DBC), date palm waste–derived biochar composite with nano-zerovalent iron (nZVI-DBC), date palm waste–derived biochar composite with silica (S-DBC), and date palm waste–derived biochar composite with zeolite (Z-DBC)

highest apparent diffusion rate constant (k_{id}) was exhibited by nZVI-DBC (2.83 [mg g^{-1}]$^{-0.5}$), followed by S-DBC (2.15 [mg g^{-1}]$^{-0.5}$), DBC (1.08 [mg g^{-1}]$^{-0.5}$), and Z-DBC (0.95 [mg g^{-1}]$^{-0.5}$), suggesting a quick adsorption of CTC onto nZVI-DBC due to interaparticle diffusion process. Hence, based on adsorption dynamics, power function, interaparticle diffusion, and Elovich models best described the adsorption kinetics of CTC onto the tested biochars. Moreover, nZVI-DBC exhibited the highest rate constants, initial adsorption rates, and apparent diffusion rate constants compared with other tested biochars.

Mechanism for CTC removal

Various kinetics and empirical models were used to understand the mechanism of CTC adsorption by using the engineered biochars. The best fitness of the Redlich–Peterson model suggested that both the Langmuir and Freundlich isotherms were applicable for the CTC adsorption data. The closeness of experimental data with Langmuir-modeled data suggested mono-layer coverage of CTC onto homogenous surface of the biochars, while the closeness with Freundlich-modeled data suggested multi-layer CTC adsorption onto the biochars onto heterogeneous surface of the material (Ahmad et al. 2018a, b). Additionally, mono- and multi-layer adsorptions were aided by the best fitness of Redlich–Peterson model, which combines the benefits of both the Langmuir and Freundlich isotherms. The porous structure of the biochars further facilitated the physical adsorption of CTC as indicated by the Dubinin–Radushkevich isotherm. However, it was noticed that the bonding energies (E) were less than 8 kJ g^{-1} for all the biochars, suggesting that ion-complexation mechanism was not involved in the adsorption process (Ho et al. 2002). This adsorption process was further supported by best fit of Temkin isotherm, which assumes chemisorption of an adsorbate onto the adsorbent. To further investigate the operating adsorption mechanism, adsorption dynamics data was used. The adsorption of CTC was well described by power function, Elovich, and interaparticle diffusion models. The best fitness of power function model (R^2

Table 3 Standard errors of estimate (SEE) of kinetic models for CTC (chlortetracycline) adsorption onto date palm waste–derived biochar (DBC), date palm waste–derived biochar composite with nano-zerovalent iron (nZVI-DBC), date palm waste–derived biochar composite with silica (S-DBC), and date palm waste–derived biochar composite with zeolite (Z-DBC)

Sorbent	First-order		Second-order		Pseudo-first-order		Pseudo-second-order		Elovich		Intraparticle diffusion		Power function	
	R^2	SEE	R^2	SEE	R^2	SEE	R^2	SEE	R^2	SEE	R^2	SEE	R^2	SEE
nZVI-DBC	0.34	0.003	0.02	0.485	0.84	4.0×10^{-5}	0.33	2.8×10^{-4}	0.89	5.8×10^{-3}	0.85	1.6×10^{-3}	0.96	2.8×10^{-5}
S-DBC	0.45	0.004	0.07	0.019	0.82	3.4×10^{-4}	0.90	1.6×10^{-4}	0.79	1.3×10^{-4}	0.94	1.9×10^{-3}	0.99	1.9×10^{-7}
Z-DBC	0.38	0.011	0.01	0.192	0.79	3.5×10^{-7}	0.98	2.7×10^{-5}	0.94	3.9×10^{-4}	0.90	1.0×10^{-3}	0.98	0.652
DBC	0.62	0.028	0.11	0.299	0.95	1.8×10^{-4}	0.70	0.010	0.56	4.4×10^{-4}	0.96	9.5×10^{-4}	0.93	5.0×10^{-5}

Table 4 Standard errors of estimate (SEE) of kinetic models for CTC (chlortetracycline) adsorption onto date palm waste–derived biochar (DBC), date palm waste–derived biochar composite with nano-zerovalent iron (nZVI-DBC), date palm waste–derived biochar composite with silica (S-DBC), and date palm waste–derived biochar composite with zeolite (Z-DBC)

Sorbent	First-order	Second-order	Pseudo-first-order		Pseudo-second-order			Elovich		Intraparticle diffusion		Power function	
	k_1	k_2	k_1'	q_e	k_2'	q_e	h	a	β	k_{id}	c	k_f	b
nZVI-DBC	3.6×10^{-3}	1.0×10^{-5}	-6.2×10^{-5}	3.83	1.0×10^{-5}	3282	5.76	11.5	−5.13	2.83	8.88	0.70	0.20
S-DBC	3.7×10^{-3}	2.0×10^{-5}	-6.2×10^{-5}	3.77	1.1×10^{-4}	62.16	0.44	7.80	−6.51	2.15	0.10	0.63	0.05
Z-DBC	2.8×10^{-5}	1.0×10^{-5}	-4.5×10^{-5}	2.65	6.2×10^{-4}	26.66	0.44	3.84	−1.53	0.95	3.15	0.52	0.11
DBC	$3.6 \times 10–^{3}$	-1.2×10^{-4}	-4.7×10^{-3}	3.15	9.7×10^{-5}	36.02	0.13	2.41	−3.60	1.08	−1.68	0.51	−0.19

ranged between 0.93 and 0.99) suggested a strong relationship between the mass of CTC adsorbed on a unit mass of the biochars and time of reaction. The R^2 values for the interaparticle diffusion model ranged between 0.85 and 0.96, indicating the heterogeneous diffusion of CTC particles into the porous surface of the biochars. Likewise, the best fitness of Elovich model (R^2 ranged between 0.56 and 0.89) suggested multi-layer chemisorption (covalent binding with the surface functional groups) as the rate-limiting step in CTC adsorption onto the tested biochars, which corresponded to the results of Freundlich and Temkin isotherms. The chemisorption process was further supported by the fitness of pseudo-second-order model to some extent (R^2 ranged between 0.33 and 0.98). Beside heterogeneous diffusion and chemisorption, the CTC

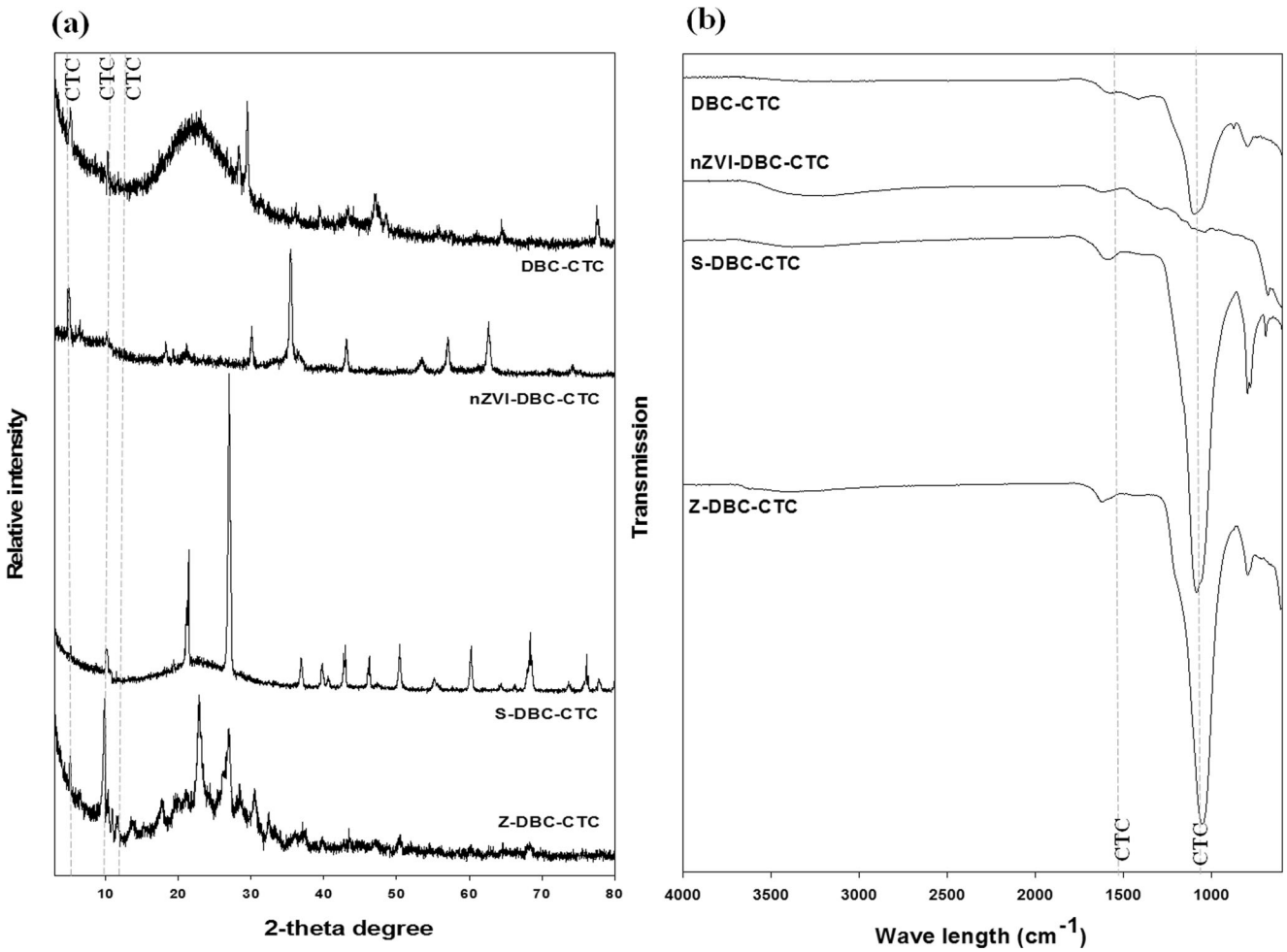

Fig. 5 **a** XRD (X-ray diffraction) and **b** FTIR (Fourier transform infrared spectroscopy) spectra after CTC (chlortetracycline) adsorption onto date palm waste–derived biochar (DBC), date palm waste–derived biochar composite with nano-zerovalent iron (nZVI-DBC), date palm waste–derived biochar composite with silica (S-DBC), and date palm waste–derived biochar composite with zeolite (Z-DBC)

adsorption was also aided by the physical adsorption onto the surfaces as described by pseudo-first-order kinetics model and Langmuir isotherm. Therefore, it was stated that the CTC adsorption onto the biochars was being controlled with multiple sorption processes including diffusion into pores, chemical reactions with the surface functional groups, and physical adsorption on the surfaces of the tested biochars. The highest adsorption of CTC onto nZVI-DBC followed by S-DBC and Z-DBC could be due to the decline in solution pH towards acidity (Fig. S4a and b), as the CTC adsorption is highly influenced by the solution pH and hydrophobicity of the sorbent (Torres-Pérez et al. 2012). The correlation of solution pH with CTC adsorption has presented a significant negative correlation with R^2 value of 0.92 (Fig. S4c). Therefore, nZVI-DBC exhibited the highest CTC adsorption due to lowest solution pH compared with other biochars. It has been observed that the maximum rise in solution pH for DBC, nZVI-DBC, S-DBC, and Z-DBC was 7.44, 5.5, 6.6, and 6.8, respectively, suggesting that the solution pH remained below the pH at point of zero charge for all the sorbents (pH_{PZC} for DBC, nZVI-DBC, S-DBC, and Z-DBC was 8.7, 5.2, 8.1, and 9.2, respectively) (Fig. S4d). These results suggested that both negative and positive surface charges were prevailing on the all the adsorbents. As the solution pH was in the range of 3.30–7.44, the protons from phenolic-pentanedione of CTC were released, which has transformed CTC into zwitterion (having both positive and negative electrical charges on different locations). Therefore, due to the presence of both negative and positive charges simultaneously on CTC, the solution pH range of 2–6 is considered to be optimum for CTC adsorption (Guocheng et al. 2012). The adsorption of CTC onto the biochars was confirmed by analyzing the post-sorption biochar samples with SEM, XRD, and FTIR. The SEM images showed whitish compounds on the surface and within the pores, which might be referred to the CTC molecules (Fig. 1f–i). Three new peaks in all the biochars detected at $2\theta = 4.28$, 10.09, and 11.86 were ascribed as CTC in XRD patterns of post-sorption biochar samples (Fig. 5a). Likewise, a small band at 1527 cm^{-1} and a shoulder peak at 1079 cm^{-1} were designated as CTC in FTIR spectra of post-sorption biochars (Fig. 5b). The variations at 1079 and 1527 suggested that some chemical interactions have occurred between amide groups of CTC with C–O–C, Si–O, and N–H groups of biochars, respectively (Zhang et al. 2015). Therefore, the CTC adsorption onto DBC, S-DBC, Z-DBC, and nZVI-DBC was being controlled by multiple mechanisms such as (i) chemical adsorption, (ii) physical adsorption (H-bonding), and porous diffusion.

It has been reported that the surface polarity of the adsorbent is of critical importance in controlling the adsorption of an organic pollutant via π-π electron donor–accepter interactions. Due to the lowest O/C ratio (0.043) of nZVI-DBC

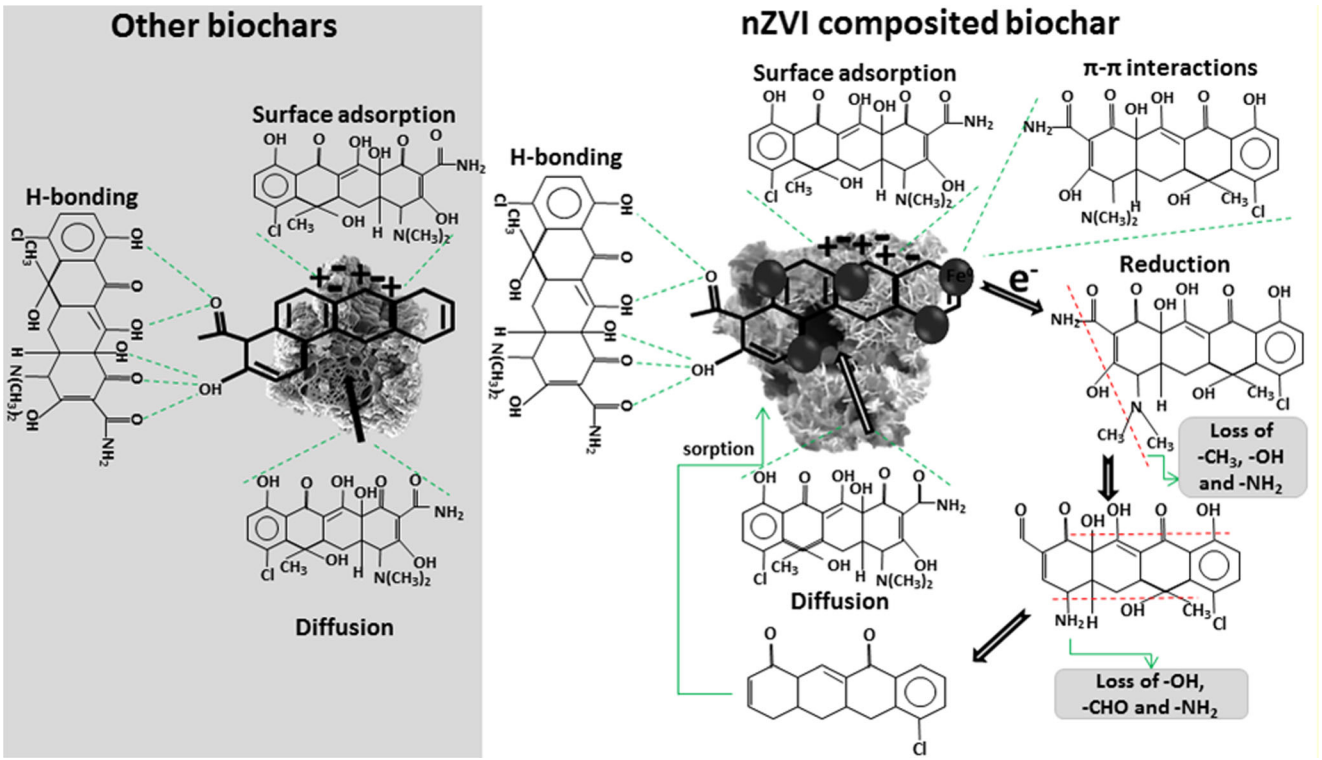

Fig. 6 Proposed mechanisms involved in CTC (chlortetracycline) adsorption onto date palm waste–derived biochar (DBC), date palm waste–derived biochar composite with nano-zerovalent iron (nZVI-DBC), date palm waste–derived biochar composite with silica (S-DBC), and date palm waste–derived biochar composite with zeolite (Z-DBC)

among all the studied sorbents and lowest pH_{PZC} (5.2), the chances of CTC adsorption onto nZVI-DBC via π-π electron donor–accepter interactions enhanced significantly. Additionally, the Fe^0 particles in the nZVI-DBC acted as reducing agent, which might adsorb the CTC molecule via π-π electron donor–accepter interactions on one hand, and reduced the CTC molecules on the other hand by removing –CH_3, –NH_2, –OH, and –CHO groups (Chen et al. 2011; Rajapaksha et al. 2015). The degraded CTC molecules after the loss of functional groups may further adsorb onto the nZVI-DBC matrix after reduction, while the Fe^0 particles were converted to Fe^{3+} and Fe^{2+} after oxidation. Additionally, the amino group in CTC may have produced Fe–N covalent bonds with Fe^{3+} and Fe^{2+} after oxidation of Fe^0, resulting in higher CTC adsorption in nZVI-DBC compared with other biochars (Zhang et al. 2015). It has been reported from the previous researches that the adsorption of the organic pollutants onto carbon-based sorbents might be controlled by π-π interaction, H-bonding, hydrophobic interaction, electrostatic interactions, and pore-filling (Swathi and Sebastian 2009; Han et al. 2014; Gao et al. 2012). Likewise, Jiang et al. (2013) stated that O-containing functional groups were responsible for higher tetracycline adsorption due to π–π electron donor–acceptor interactions. The absence of O-containing functional groups at 3426 and 1650 cm^{-1} in post-sorption sorbents confirmed the presence of π–π interactions between the sorbents and CTC (Fig. 5b). Therefore, it was concluded that (i) chemisorption, (ii) H-bonding, and (iii) diffusion into the surface pores could be the operating mechanisms controlling CTC adsorption onto DBC, S-DBC, and Z-DBC, while (i) chemisorption, (ii) H-bonding, (iii) diffusion into the surface pores, (iv) redox reactions, and (v) π-π electron donor–accepter interactions could be the operating mechanisms for CTC adsorption onto nZVI-DBC composites (Fig. 6).

Conclusion

Date palm waste–derived biochar (DBC) was used to design various engineered biochars with nZVI, silica, and zeolite (nZVI-DBC, S-DBC, and Z-DBC, respectively), and tested for chlortetracycline (CTC) removal from aqueous solutions. The produced biochars were characterized to investigate chemical, structural, and surface properties. The nZVI-DBC exhibited lowest pH (6.15) and highest surface area (220.92 $m^2\ g^{-1}$) compared with other biochars. Isotherm and kinetics batch adsorption experiments were conducted to investigate the efficiency of the produced sorbent materials for CTC removal from aqueous solutions. Langmuir-predicted maximum CTC adsorption capacity was in the order of nZVI-DBC (89.05 mg g^{-1}) > S-DBC (45.57 mg g^{-1}) > Z-DBC (30.42 mg g^{-1}) > DBC (28.19 mg g^{-1}). Kinetics adsorption data was best described by power function, interaparticle diffusion, pseudo-first-order, and Elovich models. Chemisorption, H-bonding, and porous diffusion were the main mechanisms controlling CTC adsorption onto DBC, S-DBC, and Z-DBC. However, the highest CTC removal by nZVI-DBC was resulted by the augmentation of chemisorption, H-bonding, and diffusion process with π-π electron donor–accepter interactions and redox reactions. Therefore, nZVI-DBC can be used as an efficient sorbent for cost-effective and eco-friendly removal of CTC from wastewater. Moreover, producing biochar from date palm waste through pyrolysis may reduce surface pollution. Hence, date palm–derived biochar composited with nZVI could serve as an economic and green technology for the remediation of CTC-contaminated wastewater.

Funding information This work was funded by the Dean of Scientific Research at King Saud University through research group no. RG-1439-043.

Compliance with ethical standards

Conflict of interest The authors declare that they have no conflict of interest.

References

Ahmad M, Lee SS, Rajapaksha AU, Vithanage M, Zhang M, Cho JS, Lee SE, Ok YS (2013) Trichloroethylene adsorption by pine needle biochars produced at various pyrolysis temperatures. Bioresour Technol 143:615–622

Ahmad M, Ahmad M, Usman AR, Al-Faraj AS, Abduljabbar A, Ok YS, Al-Wabel MI (2017) Date palm waste-derived biochar composites with silica and zeolite: synthesis, characterization and implication for carbon stability and recalcitrant potential. Environ Geochem Health 1–18. https://doi.org/10.1007/s10653-017-9947-0

Ahmad M, Ahmad M, Usman AR, Al-Faraj AS, Abduljabbar AS, Al-Wabel MI (2018a) Biochar composites with nano zerovalent iron and eggshell powder for nitrate removal from aqueous solution with coexisting chloride ions. Environ Sci Pollut Res 25:25757–25771

Ahmad M, Ahmad M, Usman ARA, Al-Faraj AS, Ok YS, Hussain Q, Abduljabbar A, Al-Wabel MI (2018b) An efficient phosphorus scavenging from aqueous solution using magnesiothermally modified bio-calcite. Environ Technol 39:1638–1649

Ahmad M, Usman AR, Al-Faraj AS, Ahmad M, Sallam A, Al-Wabel MI (2018c) Phosphorus-loaded biochar changes soil heavy metals availability and uptake potential of maize (Zea mays L.) plants. Chemosphere 194:327–339

Ahmaruzzaman M (2008) Adsorption of phenolic compounds on low-cost adsorbents: a review. Adv Colloid Interf Sci 143:48–67

Al-Wabel MI, Al-Omran A, El-Naggar AH, Nadeem M, Usman ARA (2013) Pyrolysis temperature induced changes in characteristics and chemical composition of biochar produced from conocarpus wastes. Bioresour Technol 131:374–379

Aly HM (2017) Biochar and its importance in adsorption of antibiotic and heavy metals from aqueous solutions. Ecol Quest 24:75–78

American Society for Testing and Materials (ASTM) (1989) Standard methods for chemical analysis of wood charcoal, ASTM D1762-84. Philadelphia, PA, USA

Ashfaq M, Khan KN, Rasool S, Mustafa G, Saif-Ur-Rehman M, Nazar MF, Sun Q, Yu CP (2015) Occurrence and ecological risk assessment of fluoroquinolone antibiotics in hospital waste of Lahore, Pakistan. Environ Toxicol Pharmacol 42:16–22

Bao Y, Zhou Q, Guan L, Wang Y (2009) Depletion of chlortetracycline during composting of aged and spiked manures. Waste Manag 29: 1416–1423

Bilgic C (2005) Investigation of the factors affecting organic cation adsorption on some silicate minerals. J Colloid Interface Sci 281:33–38

Chatterjee S, Lim SR, Woo SH (2010) Removal of reactive black 5 by zero-valent iron modified with various surfactants. Chem Eng J 160: 27–32

Chen H, Luo H, Lan Y, Dong T, Hu B, Wang Y (2011) Removal of tetracycline from aqueous solutions using polyvinylpyrrolidone (PVP-K30) modified nanoscale zero valent iron. J Hazard Mater 192:44–53

Daughton CG, Ternes TA (1999) Pharmaceuticals and personal care products in the environment agents of subtle change. Environ Health Perspect 107:907–938

Devi P, Saroha AK (2014) Synthesis of the magnetic biochar composites for use as an adsorbent for the removal of pentachlorophenol from the effluent. Bioresour Technol 169:525–531

Dong H, Deng J, Xie Y, Zhang C, Jiang Z, Cheng Y, Hou K, Zeng G (2017) Stabilization of nanoscale zero-valent iron (nZVI) with modified biochar for Cr(VI) removal from aqueous solution. J Hazard Mater 332:79–86

Foo KY, Hameed BH (2010) Insights into the modeling of adsorption isotherm systems. Chem Eng J 156:2–10

Gao Y, Li Y, Zhang L, Huang H, Hu J, Shah SM, Su X (2012) Adsorption and removal of tetracycline antibiotics from aqueous solution by graphene oxide. J Colloid Interface Sci 15:540–546

Guocheng LÜ, Limei WU, Xiaolong WANG, Libing LIAO, Xiaoyu WANG (2012) Adsorption of chlortetracycline from water by rectories. Chin J Chem Eng 20:1003–1007

Gurses A, Dogar C, Yalcin M, Acikyildiz M, Bayrak R, Karaca S (2006) The adsorption kinetics of the cationic dye, methylene blue, onto clay. J Hazard Mater 131:217–228

Han L, Sun K, Jin J, Wei X, Xia X, Wu F, Gao B, Xing B (2014) Role of structure and microporosity in phenanthrene sorption by natural and engineered organic matter. Environ Sci Ttechnol 48:11227–11234

Hao R, Xiao X, Zuo X, Nan J, Zhang W (2012) Efficient adsorption and visible-light + photocatalytic degradation of tetracycline hydrochloride using mesoporous BiOI microspheres. J Hazard Mater 209: 137–145

Hernandez-Mena L, Pecora A, Beraldo A (2014) Slow pyrolysis of bamboo biomass: analysis of biochar properties. Chem Eng Trans 37: 115–120

Ho YS, Porter JF, McKay G (2002) Equilibrium isotherm studies for the sorption of divalent metal ions onto peat: copper, nickel and lead single component systems. Water Air Soil Pollut 141:1–33

Jiang HY, Zhang DD, Xiao SC, Geng CN, Zhang X (2013) Occurrence and sources of antibiotics and their metabolites in river water, WWTPs, and swine wastewater in Jiulongjiang River basin, South China. Environ Sci Pollut Res 20:9075–9083

Joseph SD, Camps-Arbestain M, Lin Y, Munroe P, Chia CH, Hook J, Van Zwieten L, Kimber S, Cowie A, Singh BP, Lehmann J (2010) An investigation into the reactions of biochar in soil. Soil Res 48:501–515

Kumar K, Gupta SC, Baidoo KS, Chander Y, Rosen CJ (2005) Antibiotic uptake by plants from soil fertilized with animal manure. J Environ Qual 34:2082–2086

Kummerer K (2009) Antibiotics in the aquatic environment-a review-part I. Chemosphere 75:417–434

Kümmerer K, Henninger A (2003) Promoting resistance by the emission of antibiotics from hospitals and households into effluent. Clin Microbiol Infect 9:1203–1214

Lindberg RH, Fick J, Tysklind M (2010) Screening of antimycotics in Swedish sewage treatment plants-waters and sludge. Water Res 44: 649–657

Liu QS, Zheng T, Wang P, Jiang JP, Li N (2010) Adsorption isotherm, kinetic and mechanism studies of some substituted phenols on activated carbon fibers. Chem Eng J 157:348–356

Liu WJ, Zeng FX, Jiang H, Zhang XS (2011) Preparation of high adsorption capacity bio-chars from waste biomass. Bioresour Technol 102: 8247–8252

Makowska N, Koczura R, Mokracka J (2016) Class 1 integrase, sulfonamide and tetracycline resistance genes in wastewater treatment plant and surface water. Chemosphere 144:1665–1673

Meng Y, Guan B, Wu Z, Wang D (2006) Enhanced degradation of carbon tetrachloride by surfactant-modified zero-valent iron. J Zhejiang Univ Sci 7:702–707

Mohan D, Rajput S, Singh VK, Steele PH, Pittman CU Jr (2011) Modeling and evaluation of chromium remediation from water using low cost bio-char, a green adsorbent. J Hazard Mater 188:319–333

Mohan D, Sarswat A, Yong SO, Jr CUP (2014) Organic and inorganic contaminants removal from water with biochar, a renewable, low cost and sustainable adsorbent – a critical review. Bioresour Technol 160:191–202

Montforts MH (1999) Environmental risk assessment for veterinary medicinal products. Part 1: other than GMO-containing and immunological products. RIVM report 601300 001, N120. National Institute of Public Health and the Environment, Bithoven

Ok YS, Yang JE, Zhangm YS, Kim SJ, Chung DY (2007) Heavy metal adsorption by a formulated zeolite-Portland cement mixture. J Hazard Mater 147:91–96

Ozcimen D, Ersoy-Mericboyu A (2010) Characterization of biochar and bio-oil samples obtained from carbonization of various biomass materials. Renew Energy 35:1319–1324

Phenrat T, Saleh N, Sirk K, Tilton RD, Lowry GV (2006) Aggregation and sedimentation of aqueous nanoscale zerovalent iron dispersions. Environ Sci Technol 41:284–290

Rajapaksha AU, Vithanage M, Ahmad M, Seo DC, Cho JS, Lee SE, Lee SS, Ok YS (2015) Enhanced sulfamethazine removal by steam-activated invasive plant-derived biochar. J Hazard Mater 290:43–50

Rawal A, Joseph SD, Hook JM, Chia CH, Munroe PR, Donne S, Lin Y, Phelan D, Mitchell DR, Pace B, Horvat J (2016) Mineral–biochar composites: molecular structure and porosity. Environ Sci Technol 50:7706–7714

Reddy DHK, Lee S-M (2014) Magnetic biochar composite: facile synthesis, characterization, and application for heavy metal removal. Colloids Surf A Physicochem Eng Asp 454:96–103

Redlich OJDL, Peterson DL (1959) A useful adsorption isotherm. J Phys Chem 63:1024–1024

Richard LA (1954) Diagnoses and improvement of saline and alkali soils. Agriculture handbook, vol 60. USDA, USA

Simazaki D, Kubota R, Suzuki T, Akiba M, Nishimura T, Kunikane S (2015) Occurrence of selected pharmaceuticals at drinking water purification plants in Japan and implications for human health. Water Res 76:187–200

Singh R, Misra V, Singh RP (2011) Synthesis, characterization and role of zero-valent iron nanoparticle in removal of hexavalent chromium from chromium-spiked soil. J Nanopart Res 13:4063–4073

Singh S, Shukla S, Tandia N, Kumar N, Paliwal R (2014) Antibiotic residues: a global challenge. Pharma Sci Monitor 5

Sun Y, Gao B, Yao Y, Fang J, Zhang M, Zhou Y, Chen H, Yang L (2014) Effects of feedstock type, production method, and pyrolysis temperature on biochar and hydrochar properties. Chem Eng J 240:574–578

Swathi RS, Sebastian KL (2009) Long range resonance energy transfer from a dye molecule to graphene has (distance)(-4) dependence. J Chem Phys 130:086101

Torres-Pérez J, Gérente C, Andrès Y (2012) Sustainable activated carbons from agricultural residues dedicated to antibiotic removal by adsorption. Chin J Chem Eng 20:524–529

Uchimiya M, Bannon DI, Wartelle LH (2012) Retention of heavy metals by carboxyl functional groups of biochars in small arms range soil. J Agric Food Chem 60:1798–1809

Usman AR, Abduljabbar A, Vithanage M, Ok YS, Ahmad M, Ahmad M, Elfaki J, Abdulazeem SS, Al-Wabel MI (2015) Biochar production from date palm waste: charring temperature induced changes in composition and surface chemistry. J Anal Appl Pyrol 115:392–400

Wang Y, Lu H, Liu Y, Yang S (2016) Removal of phosphate from aqueous solution b SiO2 –biochar nanocomposites prepared by pyrolysis of vermiculite treated algal biomass. RSC Adv 6:83534–83546

Wang B, Jiang YS, Li FY, Yang DY (2017) Preparation of biochar by simultaneous carbonization, magnetization and activation for norfloxacin removal in water. Bioresour Technol 233:159–165

Xu J, Gao N, Tang Y, Deng Y, Sui M (2010) Perchlorate removal using granular activated carbon supported iron compounds: synthesis, characterization and reactivity. J Environ Sci 22:1807–1813

Yang H, Yan R, Chen H, Lee DH, Zheng C (2007) Characteristics of hemicellulose, cellulose and lignin pyrolysis. Fuel 86:1781–1788

Yao Y, Gao B, Chen J, Yang L (2013) Engineered biochar reclaiming phosphate from aqueous solutions: mechanisms and potential application as a slow-release fertilizer. Environ Sci Technol 47:8700–8708

Zhang Z, Lan H, Liu H, Qu J (2015) Removal of tetracycline antibiotics from aqueous solution by amino-Fe (III) functionalized SBA15. Colloids Surf A Physicochem Eng Asp 471:133–138

Zhao X, Shi Y, Cai Y, Mou S (2008) Cetyltrimethylammonium bromidecoated magnetic nanoparticles for the preconcentration of phenolic compounds from environmental water samples. Environ Sci Technol 42:1201–1206

Zhou Q, Li Z, Shuang C, Li A, Zhang M, Wang M (2012) Efficient removal of tetracycline by reusable magnetic microspheres with a high surface area. Chem Eng J 210:350–356